Trace and minor elements in sphalerite from metamorphosed sulphide deposits

ARTICLE *in* MINERALOGY AND PETROLOGY · DECEMBER 2014

Impact Factor: 1.35 · DOI: 10.1007/s00710-014-0346-2

3 AUTHORS, INCLUDING:

Nigel J Cook
University of Adelaide
163 PUBLICATIONS **2,032** CITATIONS
SEE PROFILE

Cristiana L. Ciobanu
University of Adelaide
97 PUBLICATIONS **1,309** CITATIONS
SEE PROFILE

Miner Petrol (2014) 108:873–890
DOI 10.1007/s00710-014-0346-2

ORIGINAL PAPER

Trace and minor elements in sphalerite from metamorphosed sulphide deposits

Julian A. Lockington · Nigel J. Cook · Cristiana L. Ciobanu

Received: 11 January 2014 / Accepted: 30 July 2014 / Published online: 12 August 2014

Abstract Sphalerite is a common sulphide and is the dominant ore mineral in Zn-Pb sulphide deposits. Precise determination of minor and trace element concentrations in sulphides, including sphalerite, by Laser-Ablation Inductively-Coupled-Plasma Mass-Spectrometry (LA-ICP-MS) is a potentially valuable petrogenetic tool. In this study, LA-ICP-MS is used to analyse 19 sphalerite samples from metamorphosed, sphalerite-bearing volcanic-associated and sedimentary exhalative massive sulphide deposits in Norway and Australia. The distributions of Mn, Fe, Co, Cu, Ga, Se, Ag, Cd, In, Sn, Sb, Hg, Tl, Pb and Bi are addressed with emphasis on how concentrations of these elements vary with metamorphic grade of the deposit and the extent of sulphide recrystallization. Results show that the concentrations of a group of trace elements which are believed to be present in sphalerite as micro- to nano-scale inclusions (Pb, Bi, and to some degree Cu and Ag) diminish with increasing metamorphic grade. This is interpreted as due to release of these elements during sphalerite recrystallization and subsequent remobilization to form discrete minerals elsewhere. The concentrations of lattice-bound elements (Mn, Fe, Cd, In and Hg) show no correlation with metamorphic grade. Primary metal sources, physico-chemical conditions during initial deposition, and element partitioning between sphalerite and co-existing sulphides are dominant in defining the concentrations of these elements and they appear to be readily re-incorporated into recrystallized sphalerite, offering potential insights into ore genesis. Given that sphalerite accommodates a variety of trace elements that can be precisely determined by contemporary microanalytical techniques, the mineral has considerable potential as a geothermometer, providing that element partitioning between sphalerite and coexisting minerals (galena, chalcopyrite etc.) can be quantified in samples for which the crystallization temperature can be independently constrained.

Editorial handling: A. Beran

J. A. Lockington · N. J. Cook (✉) · C. L. Ciobanu
Centre for Tectonics, Resources and Exploration (TRaX), School of Earth and Environmental Sciences, University of Adelaide, Adelaide, S.A. 5005, Australia
e-mail: nigel.cook@adelaide.edu.au

Introduction

Zinc sulphide (ZnS) occurs naturally in three forms, sphalerite, wurtzite and (rare) matraite. Of these, sphalerite, composed of Zn and S atoms arranged in a tetrahedral coordination within a face-centred cubic lattice, is by far the most common. Sphalerite is the main ore for zinc and the dominant mineral in most types of zinc sulphide deposits, including epithermal vein systems, skarns, volcanic-hosted massive sulphides (VHMS), sedimentary-exhalative (SEDEX), and Mississippi-Valley-Type (MVT) deposits.

Sphalerite can incorporate iron and a wide range of minor and/or trace elements, locally in concentrations that are economic to recover, such as germanium (Ge) or indium (In), or which pose environmental and/or processing problems, such as cadmium (Cd) or manganese (Mn) (Cook et al. 2009a and references therein). As well as potentially influencing the economic value of a zinc sulphide deposit, the distribution of minor/trace elements in sphalerite can be an important source of petrographic information, especially for identifying processes of ore genesis or source (Cook et al. 2009a; Ye et al. 2011).

Laser-ablation inductively coupled plasma mass-spectrometry (LA-ICP-MS) is established as an efficient and accurate method for analysis of trace element distributions in sulphides (e.g. Fryer et al. 1995). The availability of matrix-matched sulphide standards (e.g. Wilson et al. 2002; Danyushevsky et al. 2011) allows for sub-ppm precision and

good accuracy. As a result, published trace element compositional data for sphalerite and other sulphides has expanded rapidly. Iron is the most common minor element in sphalerite, commonly at wt.% concentrations as in sphalerite analysed here. Partial solid solution exists between FeS and ZnS; up to 56 mol% FeS can replace ZnS under laboratory conditions (Vaughan and Craig 1978). Manganese and Cd substitutions extend to around 15 and 14 mol% MnS and CdS, respectively (Tauson et al. 1977; Pattrick et al. 1998). Manganese is a relatively common component of sphalerite, yet published data sets show that there is a broad variation in concentrations in different sphalerite samples, ranging from trace amounts to several wt.%; in some epithermal deposits MnS concentrations can exceed 5 % (Cook et al. 2009a). Manganese incorporation into sphalerite occurs via cation exchange ($Zn^{2+} \leftrightarrow Mn^{2+}$). Alabandite (MnS) is, however, not isostructural with sphalerite and there is an upper limit to incorporation (~7 mol% Mn (Sombuthawee et al. 1978)).

Multi-deposit studies of trace element distributions in sphalerite have demonstrated consistent distribution patterns in ores of different types (Cook et al. 2009a; Ye et al. 2011; Murakami and Ishihara 2013). Cobalt and indium, for example, are generally concentrated in sphalerite from relatively high-temperature hypothermal and mesothermal ore deposits. In contrast, enrichment in Ga, Ge and Hg is noted in sphalerite from lower temperature epithermal ores. Sphalerite from epithermal, intrusion-related or sediment-hosted ore systems commonly displays compositional zoning, expressed as oscillatory bands of sphalerite enriched in a specific element or elements (Pattrick et al. 1993; Beaudoin 2000; Di Benedetto et al. 2005; Barrie et al. 2009).

Relatively little attention has been given to the fate of trace elements in sphalerite upon regional metamorphism, associated deformation, remobilization and sulphide recrystallization, whether during the prograde or retrograde portions of the metamorphic cycle. This is in contrast to other common sulphides, particularly pyrite and arsenopyrite, in which the effects of regional metamorphic overprinting on sulphide mineral chemistry, especially the distribution of gold in the crystal lattice and as nano- to micron-sized inclusions, have been documented in some detail (e.g. Mumin et al. 1994; Larocque et al. 1995; Oberthür et al. 1997; Genkin et al. 1998; Wagner et al. 2007; Morey et al. 2008; Cook et al. 2009b, 2013; Large et al. 2009; Ciobanu et al. 2012; Deol et al. 2012). Sulphide recrystallization will generally result in certain trace elements being released from the host, either by fluid-assisted or diffusional processes, whereas other elements will be reincorporated in the lattice. Syn-metamorphic recrystallization may also result in homogenization of mineral compositions, with any compositional zoning either reflecting in primary signatures in non-recrystallized relics, or sub-solidus diffusional processes. Sulphur isotopes display similar patterns; recrystallized sulphides generally, though not exclusively, display tightly clustered $\delta^{34}S$ values indicating homogenization (e.g. Cook and Hoefs 1997).

In this contribution, we present compositional data for sphalerite in six deposits in the Norwegian Caledonides and Australia (Table 1, Fig. 1) which have undergone metamorphism at peak conditions ranging from greenschist to granulite facies, and in which we recognise sulphide recrystallization. By comparing element distributions in sphalerite from the different deposits we aim to identify the possible effects of burial metamorphism on sphalerite trace element chemistry. Trace element partitioning is a function of (i) the speciation of co-existing phases and their K_D values for the respective trace elements, and (ii) trace element release/incorporation during cycles of prograde and retrograde re-crystallisation. In this work, we also explore the inter-element relationships in sphalerite.

The selection of deposits encompasses sulphide assemblages that are all, except Mt Isa, characterised by exotic trace mineralogy implying peculiar geochemical signatures in the primary, syn-depositional ores. Moreover, the Norwegian Caledonides represent a metallogenetic belt in which exotic Pb-Ag-Sb-As-sulphosalt mineralogy has been used to fingerprint remobilisation, a phenomenon recognizable at scales ranging from the hand specimen to orefield (e.g. Vokes 1976; Cook 1996; Cook et al. 1998; Spry et al. 2000).

Deposit background

Norwegian samples

Investigated Norwegian samples derive from deposits in the Scandinavian Caledonides (Roberts and Gee 1985), a belt of late Precambrian to early Palaeozoic rocks emplaced as a series of nappes onto the Fennoscandian basement. These rocks were variably deformed and metamorphosed during the Caledonian Orogeny and outcrop as a series of nappes and thrust sheets along the Western margin of the Scandinavian Peninsula. The Caledonides host numerous VHMS- and SEDEX-style sulphide deposits (Ihlen et al. 1997; Grenne et al. 1999; Vokes et al. 2003), which were important economic resources for Cu, and to a lesser extent, Zn-Pb, until the mid-1980's (Vokes 1976; Bugge 1978). Mineralogy and ore textures are broadly comparable from deposit to deposit (Craig and Vokes 1992). Samples were taken from the Sulitjelma, Bleikvassli and Mofjellet deposits, as well as representative sulphide bodies in the Røros district. Table 1 provides key information on each deposit, including metamorphic history.

The Sulitjelma Cu-Zn orefield (Cook et al. 1990, 1993; Cook 1996), central-north Norway, hosts over 20 massive sulphide bodies totalling around 35 Mt. The sulphide bodies are dominantly, though not exclusively, located at the contact between the Otervatn Volcanic Formation, a dominantly

Table 1 Summary of samples investigated

Deposit	Type	Peak metamorphic conditions	Samples	Sample location	Mineralogy (in order of abundance)	Textures (% sulpides)	References
Norway							
Sulitjelma	VHMS	Amphibolite facies (540 °C, 6.0 kbar)	NC5835	Giken II orebody	Py>Sp>Cp	Massive (>85)	Cook et al. (1990, 1993); Cook (1996)
			NC6005	Sagmo orebody	Py>Po>Cp>Sp	Massive (70)	
			Su 1b	Giken II orebody	Py>Sp>Cp	Massive (95)	
			Su2a	Giken II orebody	Py>Sp>Cp	Massive (95)	
			Su2b	Giken II orebody	Py>Sp>Cp	Massive (95)	
Bleikvassli	SEDEX	Upper amphibolite—lower granulite facies (570 °C, 7.5–8.0 kbar)	Bv1	Main orebody (lower)	Py>Po>Sp>Cp>Gn	Massive (70)	Vokes (1963); Cook (1993); Cook et al. (1998); Rosenberg et al. (1998)
			V59.197	Main orebody (upper)	Py>Sp>Po>Gn>Cp>Tet	Massive (95)	
			V60.446	Main orebody (upper)	Py>Sp>Po>Gn>Cp>Tet	Massive (70)	
			V61.538	Main orebody (upper)	Py>Sp>Po>Gn>Cp>Tet	Massive (70)	
Mofjellet	SEDEX (?)	Amphibolite facies (550 °C, 7.0 kbar?)	Mo2	Main orebody	Py>Cp>Sp>Po	Semi-massive (50)	Saager (1967); Bjerkgård et al. (2001); Cook (2001)
			Mo5	Main orebody	Py>Cp>Sp>Po>Tet	Semi-massive (50)	
			Mo10	Main orebody	Py>Cp>Sp>Po	Semi-massive (50)	
Røros	VHMS	Upper greenschist to lower amphibolite facies	STO 175-04	Kongens Gruve	Py>Po>Cp>Sp>Gn	Massive (70)	Bjerkgård et al. (1999); Barrie et al. (2010a)
			STO-175-06	Nye Storwartz	Py>Po>Cp>Sp>Gn	Massive (70)	
			STO 175-07	Klingenberg	Py>Po>Cp>Sp>Gn	Massive (70)	
Australia							
Mt. Isa	SEDEX (?)	Greenschist facies	5984A	Unknown	Py>Sp>Gn>Cp	Banded (50)	Painter et al. (1999); Large et al. (2005)
			5984B	Unknown	Py>Sp>Gn>Cp	Banded (50)	
Broken Hill	SEDEX (?)	Granulite facies (750–800 °C, 5–6 kbar)	BH218	Unknown	Gn>Sp>Py>Cp>Po	Massive (>85)	Haydon and McConachy (1987); Parr and Plimer (1993); Plimer (2007); Spry et al. (2000)
			BH221	Unknown	Gn>Sp>Py>Cp>Po	Massive (>85)	

Mineral abbreviations: *Cp* chalcopyrite, *Gn* galena, *Po* pyrrhotite, *Py* pyrite, *Sp* sphalerite, *Tet* tetrahedrite-tennantite

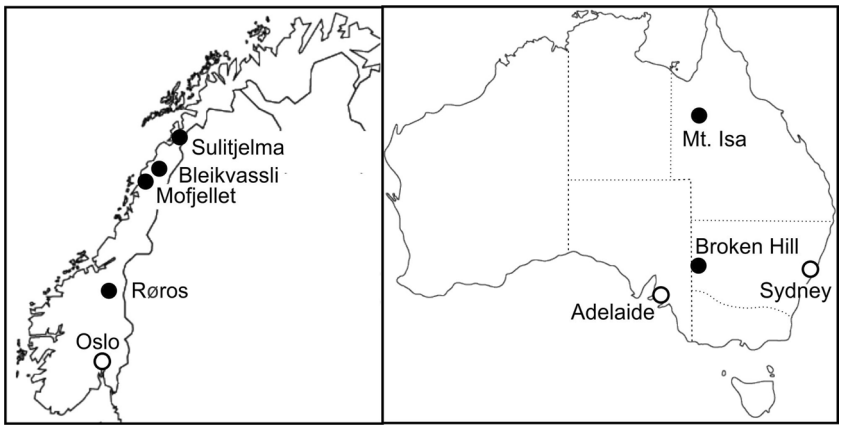

Fig. 1 Sketch maps showing the locations of deposits sampled and analysed in this study

basaltic sequence, and the overlying metasedimentary Furulund Group; see Boyle and Westhead (1992) for discussion of the geology and metamorphism of the district. The stratiform, stratabound sulphides formed as a single stratigraphic interval via chemical exhalative precipitation of hydrothermal fluids onto the seafloor from hydrothermal vents. Deposit geochemistry is consistent with convective circulation of heated seawater and leaching of subjacent mafic volcanic rocks. Amphibolite facies regional metamorphism and accompanying deformation modified the geometry of individual sulphide lenses and their spatial relationships with associated alteration (Cook et al. 1990). Isoclinal folding led to stacking of mineralized horizons within the stratigraphy; multiple sulphide bodies are arranged *en-echelon* within each horizon (Cook et al. 1993).

The Bleikvassli deposit, ~45 km southeast of Mo i Rana, was mined between 1957 and 1997, producing ~5.0 Mt of ore (4.0 % Zn, 2 % Pb, 0.15 % Cu and 25 g/t Ag). The main orebody is made up of interlayered lenses of massive sulphide ore hosted by amphibolites, quartzites, mica schists and quartzo-feldspathic gneisses of the Uppermost Allochthon (Ramberg 1967; Stephens et al. 1985; Bjerkgård et al. 1995). Most researchers consider the deposit to be of SEDEX-type (Vokes 1963, 1966; Skauli et al. 1992a, b; Moralev et al. 1995; Cook et al. 1998). The deposit underwent Caledonian metamorphism at peak conditions of ~570 °C and 7.5–8 kbar (Cook 1993; Rosenberg et al. 1998). At least five phases of syn-metamorphic deformation are recognized (Bjerkgård et al. 1995). A distinct pyrrhotite-rich ore, usually with abundant chalcopyrite, and often displaying a brecciated texture with numerous, generally rounded, clasts of wall-rock and vein quartz, occurs close to the footwall in the southern part of the deposit. Remobilization of ore components is abundant. Characteristic 'wall rock mineralization' hosts coarse Pb-As-(Sb)-sulphosalt-dominant assemblages emplaced in crosscutting veins adjacent to massive ore (Vokes 1963; Cook et al. 1998).

The Mofjellet deposit, 1 km south of Mo i Rana, is hosted within metapelitic quartz-mica-feldspar gneisses and amphibolites of the Mofjellet Group in the Rødjngsfjellet Nappe complex, Uppermost Allochthon (Saager 1967; Bjerkgård et al. 2001). The Mofjell deposit was exploited between 1926 and 1987, producing 4.3 Mt of ore grading 3.61 % Zn, 0.71 % Pb, 0.31 % Cu, as well as sulphuric acid from pyrite. Like Bleikvassli, the Mofjell deposit is interpreted as SEDEX-type (Grenne et al. 1999; Bjerkgård et al. 2001). The deposit consists of three stratiform lenses metamorphosed at lower amphibolite facies conditions (approx 550 °C and 7 kbar; Bjerkgård et al. 2001). The presence of gold was confirmed during exploration work carried out since 1990. Sulphide recrystallization and mobilization of minor elements are widespread. Sulphosalt-rich remobilizate assemblages are noted as thin veinlets within host rock immediately adjacent to massive pyrite ore (Cook 2001).

Deposits of the Røros region, Southeastern Trondheim region, are hosted within a Cambrian to Silurian turbiditic succession within the Meråker Nappe (part of the Trondheim Nappe Complex; Roberts and Wolff 1981; Gee and Sturt 1985). The district, and the several dozen contained sulphide bodies, underwent deformation and metamorphism at lower greenschist to lower amphibolite facies during Scandian orogenesis (Grenne et al. 1999; Vokes et al. 2003). VHMS deposits of the Røros district were exploited from 1644 to 1977, producing ~6.5 Mt of ore @ 2.7 % Cu, 4.2–5.0 % Zn; Bjerkgård et al. 1999. Kongens Gruve, Nye Storwartz and Klingenberg are among the largest and were studied by us. These deposits are associated with Late Ordovician calcareous phyllites, metagraywackes, and local interlayers of possible volcanoclastic origin, forming part of a large, complexly folded synformal structure (Wolff 1967; Rui 1972; Roberts and Wolff 1981; Grenne et al. 1999; Bjerkgård et al. 1999). The Røros deposits contain a diversity of ore textures, reflecting variations in pyrite:pyrrhotite ratios and gangue mineralogy.

Barrie et al. (2010a) showed that plastic strain is widespread in pyrite from the Røros District and that the more visible brittle deformation is a response to later, post-peak metamorphic conditions. In a broader study of seven

metamorphosed deposits in the Norwegian Caledonides, including the four investigated in the present study, Barrie et al. (2010b) showed that pyrite is more ductile than generally inferred, and that ductile deformation takes place even under greenschist facies conditions.

Australian samples

Samples were studied from the giant Pb-Zn deposits at Broken Hill, New South Wales, and from Mt. Isa, Queensland (Table 1). Both sample suites derive from the University of Adelaide Geology and Geophysics teaching collection; precise locations within the deposits are unknown.

The >300 Mt Broken Hill Pb-Zn-Ag deposit, South-eastern Australia, is hosted by Early to Middle Proterozoic metasedimentary and -volcanic rocks of the Willyama Supergroup in the south-eastern part of the Curnamona Craton (Haydon and McConachy 1987). These rocks comprise a range of metamorphic lithologies, including pelitic, quartzofeldspathic and mafic rocks (Pidgeon 1967; Haydon and McConachy 1987) deposited in a continental back-arc environment at ca. 1,710–1,640 Ma, and subsequently deformed during the Olarian Orogeny ca. 1,600–1,580 Ma (Stevens et al. 1988; Stüwe and Ehlers 1997). Sedimentary Adelaidian rocks (ca. 820–750 Ma) were unconformably deposited onto the metamorphic basement during break-up of Rodinia. Both the Adelaidian and Willyama Supergroups then underwent deformation during the Delamerian Orogeny (520–500 Ma).

There is a substantial literature on ore genesis at Broken Hill (Greenfield et al. 2003; Webster 2006; Spry et al. 2008 and references therein). Parr and Plimer (1993) and Phillips et al. (1985) argue that deposition of the Broken Hill ore deposit was coeval with bimodal felsic–mafic volcanism and pre-metamorphic alteration. The favoured SEDEX model (Stanton and Russell 1959; Both and Rutland 1976; Laing et al. 1978; Plimer 1979, 2007; Parr and Plimer 1993; Spry et al. 2007) therefore encompasses formation via hydrothermal processes and subsequent multi-phase high-grade metamorphism and deformation. Granulite facies metamorphism of the Broken Hill deposit led to recrystallization of ore and host rock.

An alternative model involving syntectonic introduction of metals during peak metamorphism or post-tectonic replacement has been proposed (e.g. Stillwell 1959; Nutman and Ehlers 1998; Rothery 2001). A second alternative model considers metamorphic melting of a primary sediment-hosted mineralization (Lawrence 1967; Mavrogenes et al. 2001). Mavrogenes et al. (2001) and Frost et al. (2002, 2005) argue for extensive melting of sulphides. Spry et al. (2008) suggest that although there may have been localized partial melting in minor parts of the ore, there was no substantial liquidation of the sulphides during metamorphism.

The stratiform, sediment-hosted Mt. Isa Zn-Pb-(Cu) deposit (Grondijis and Schouten 1937; Mathias and Clark 1975; Perkins 1984, 1997) lies within the Mt Isa Inlier, Western Queensland. The Mt. Isa Inlier, a multiply deformed terrane in which basement rocks are overlain by thick successions of volcanic and sedimentary rocks (Page and Sweet 1998), is part of the larger Mt. Isa-McArthur basin system which contains a number of major sulphide deposits (totalling >370 Mt @ 10 % Zn, 5.6 % Pb, and 120 g/t Ag; Large et al. 2005).

The stratiform orebodies making up the Mt. Isa deposit are hosted by reduced, fine-grained carbonaceous and pyrite-bearing Middle Proterozoic lithologies within the within the upper 650 m of the 1,000-m-thick Urquhart Shale, part of the larger Mount Isa Group (e.g. Painter et al. 1999). The Urquhart Shale underwent greenschist facies metamorphism (Large et al. 2005), and up to six phases of deformation (Bell and Hickey 1998).

Like other deposits in the Mt Isa-McArthur basin, Mt. Isa has been classified as a syngenetic SEDEX-style deposit (Knight 1953; Stanton 1963; Finlow-Bates and Stumpfl 1985; McGoldrick and Keays 1990; Smith 2000; Large et al. 2005). Despite this, there has been debate concerning genetic relationships between Zn-Pb and Cu-dominant ores. A syn-deformational replacement model for the limited volume of Cu-rich ores was advanced (Perkins 1984; Perkins and Bell 1998), and was, in part, further substantiated by Wilde et al. (2006). The deposit experienced the same sequence of metamorphism and deformation as its host rocks, substantially modifying ore textures (Stanton 1964; Perkins and Bell 1998). Perkins (1997) re-evaluated evidence for large-scale remobilization and recrystallization (e.g. McClay 1979) in terms of a single syngenetic episode of sulphide deposition in which replacement was controlled by pre-existing structures.

Chronostratigraphic correlations between the Broken Hill and the Mt. Isa-McArthur regions have been proposed (Page et al. 2005), carrying implications for the depositional and metallogenic histories of both regions. The controlling role of basinal structures on metal source(s) and flow regimes has implications for the Zn-Pb deposits and for uranium mineralization in the Mt. Isa region (Polito et al. 2006; Southgate et al. 2006).

Mineralogy and petrography

Significant textural variation is observed among samples from individual deposits. A common feature of sphalerite is the lack of compositional zoning observable either optically or in back-scattered electron images. Petrographic aspects of the sample suite are illustrated in Figs. 2 and 3.

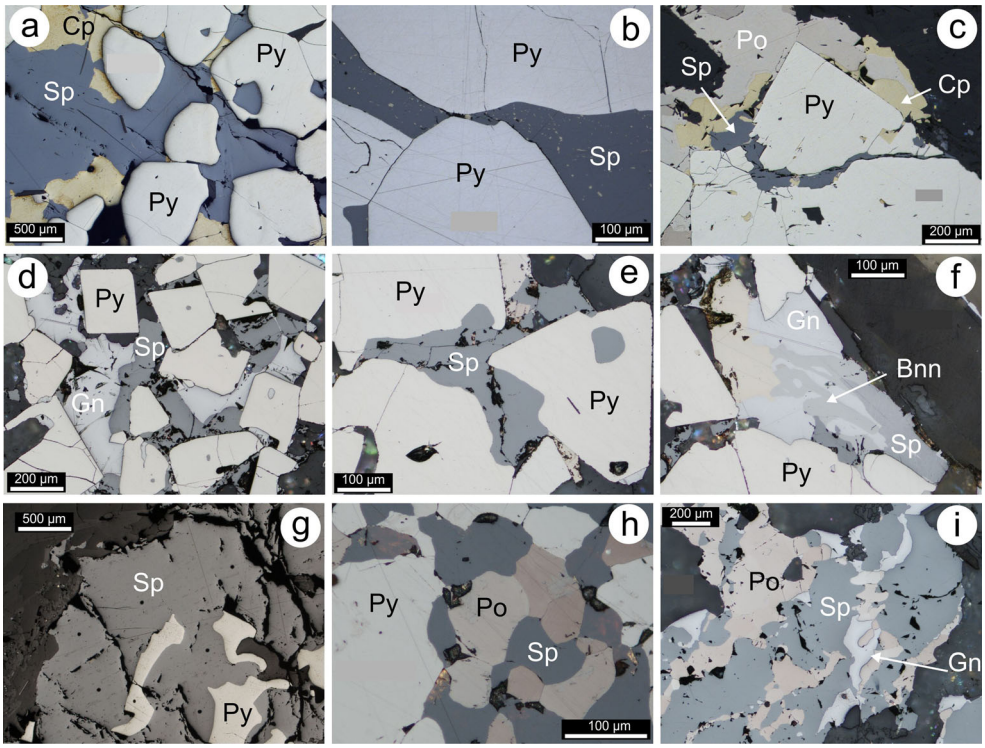

Fig. 2 Reflected light photomicrographs showing petrographic aspects of the Norwegian samples: Sulitjelma (**a**–**c**); Bleikvassli (**d**–**f**); Mofjellet (**g**); and Røros (**h**–**i**). **a** Corroded pyrite metablasts in a matrix of chalcopyrite and sphalerite. **b** Detail of sphalerite, containing chalcopyrite disease, between corroded pyrite. **c** Remobilized sphalerite filling fractures in brittle-deformed pyrite. **d** Sphaerite-galena forming the matrix to metablastic pyrite. **e** Curved boundaries between sphalerite and corroded pyrite. **f** Intergrown galena-bournonite-sphalerite. **g** Relictic, corroded pyrite in coarser sphalerite. **h** Equilibrium (?) assemblage of pyrite, pyrrhotite and sphalerite. **i** Possible replacement of sphalerite by pyrrhotite. *Abbreviations*: *Bnn* bournonite, *Cp* chalcopyrite, *Gn* galena, *Po* pyrrhotite, *Py* pyrite, *Sp* sphalerite

Norwegian sample suite

The **Sulitjelma** ores are widely cited as spectacular examples of the effects of deformation on sulphide assemblages. These include *durchbewegt* textures (Vokes 1969), involving milling of refractory sulphides such as pyrite within matrices of ductile sulphides, plastic deformation of giant pyrite porphyroblasts and shearing along the ore horizons producing sulphide mylonites (Cook et al. 1990). Syn-metamorphic sulphide recrystallization led to remobilization and local

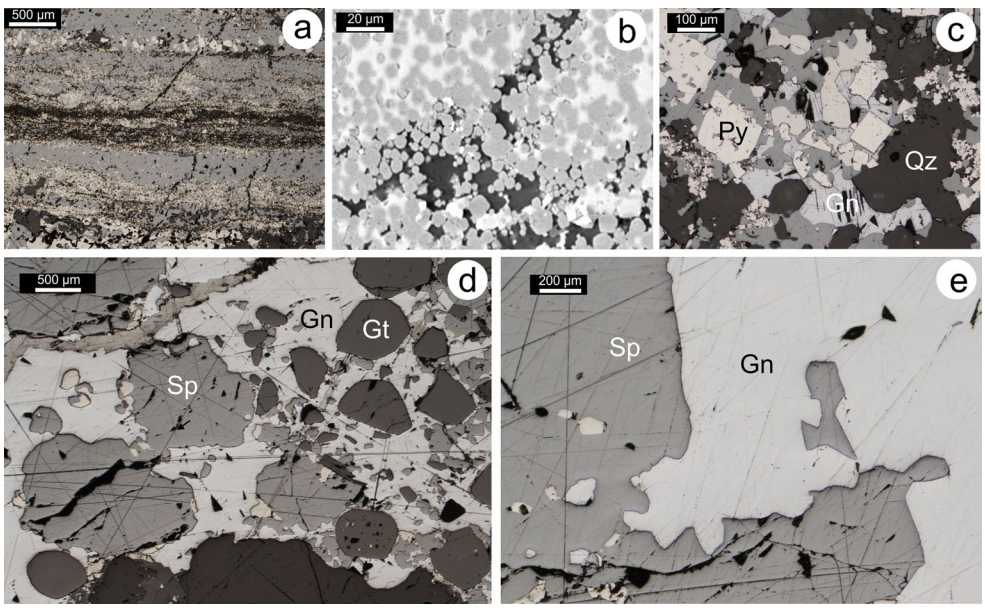

Fig. 3 Reflected light photomicrographs (except **b**, back-scatter electron image) showing petrographic aspects of samples from Mt. Isa (**a**–**c**) and Broken Hill (**d**–**e**). **a** Typical laminated texture defined by bands, tens to hundreds of µm in thickness, with varying grain size (especially of pyrite) and mineral composition, with sphalerite (*grey*) forming the rock matrix; darker bands are fine-grained quartz and calcite. **b** Detail of finely-banded pyrite-sphalerite ore comprising µm–sized, rounded pyrite in a sphalerite matrix. **c** Euhedral pyrite in matrix of sphalerite and minor galena from coarser sulphide band. **d** Sphalerite–galena ore. Sphalerite occurs as corroded relics within galena. **e** Detail showing corroded, curvilinear grain boundary between sphalerite and galena. *Gt* garnet, *Qz* quartz; other abbreviations as Fig. 2

redistribution of trace elements, including precious metals (Cook 1992, 1994, 1996). Sphalerite occurs, together with chalcopyrite and pyrrhotite, in the sulphide matrix between coarse pyrite and has been deformed in both the brittle and ductile fields. Remobilized sphalerite also fills fractures in refractory pyrite (Cook 1994).

The studied samples are coarse-grained massive sulphide ores (>50 % sulphide), dominated by up-to-cm-size pyrite and generally more chalcopyrite than sphalerite. Inter- and intragranular fracturing is observed; fractures crosscut pyrite, sphalerite and pyrrhotite. Pyrite displays fabrics indicating sequences of corrosion, recrystallization and deformation in both brittle and ductile fields (Fig. 2a–c). The influence of the host minerals is evident with pyrite generally appearing more rounded where enclosed by chalcopyrite and sphalerite. The latter sulphides fill fractures in pyrite and comprise the matrix between pyrite grains. Deformation lamellae are absent in the base metal sulphides but are commonly observed in associated pyrrhotite. Sphalerite contains abundant 'chalcopyrite disease' (Barton and Bethke 1987) (Fig. 2b).

Massive ores from **Bleikvassli** are medium-grained (mm-scale) and comprise assemblages of pyrite-sphalerite-galena ± pyrrhotite ± chalcopyrite. Base-metal sulphides and pyrrhotite occupy the matrix between pyrite metablasts (Vokes 1963). In the sample suite analysed here, pyrite and pyrrhotite are both present, the former as coarse recrystallized porphyroblastic pyrite. Some of the larger pyrite grains are crosscut by fractures. Sphalerite, pyrrhotite, chalcopyrite and galena comprise the matrix between coarse pyrite (Fig. 2d, e). Small amounts of tetrahedrite-tennantite and bournonite occur, generally forming symplectites with galena (Fig. 2f).

Samples from **Mofjellet** are massive, medium- to coarse-grained. Pyrite and sphalerite reach up to several mm in size; both display euhedral to subhedral crystal morphologies and regular to irregular grain boundaries. Lesser amounts of pyrrhotite, galena and tetrahedrite are noted in these samples, although (Cu)-Pb-Sb-(As)-sulphosalts are abundant in parts of the deposit. Textures are interpreted in terms of complete recrystallization during peak metamorphism, extensive replacement of one sulphide by another (Fig. 2g), and post-peak brittle fracture.

The samples from **Røros** are also coarse-grained and all sulphides display irregular grain margins. Pyrrhotite is the most abundant sulphide in all samples investigated; pyrite is a minor component of some and is generally restricted to relics within pyrrhotite. Textures are suggestive of recrystallization at equilibrium (Fig. 2h) but locally with some replacement between sphalerite and pyrrhotite resulting in mutual boundaries with 'carries textures' (Fig. 2i). Fabrics are consistent with deformation and possible 'flow' of the more ductile sulphides. Patches of chalcopyrite-sphalerite associated with fine-grained native bismuth are observed within quartz.

Australian sample suite

Sphalerite in the **Mt. Isa** samples is generally finer-grained than in the other deposits (Fig. 3a). On the hand specimen scale, the Mt Isa samples display semi-regular, mm- to cm-scale layering of light and dark bands which differ in composition and grain size. The banding is interpreted as syn-sedimentary banding rather than a metamorphic fabric. Sulphide mineralogy is dominated by pyrite, sphalerite and galena; gangue is dominantly quartz. The finest grained pyrite is however typically rounded and cemented by sphalerite (Fig. 3b), possibly suggesting its deposition and growth as framboids. In the coarser bands, pyrite is commonly euhedral and is often observed overgrown by co-existing sphalerite (Fig. 3c). There is little evidence in support of extensive syn-metamorphic recrystallization.

Sulphides in the **Broken Hill** samples (pyrite, galena and sphalerite) are invariably coarse-grained. There are extensive signs of replacement of sphalerite by galena, with the former occurring as relicts in the latter (Fig. 3d). The 'carries texture' shown by mutual curvilinear boundaries between the two sulphides (Fig. 3e), suggest however local equilibrium attained during recrystallization. These ores have extensively recrystallized; late, crosscutting fractures are observed across all sulphides. Metamorphic garnet, although enclosed within sulphide assemblages, also contains sulphide inclusions.

Methodology

Each sample was examined using optical and scanning electron microscopy in back-scatter electron mode to identify and characterize textures, the presence of compositional zoning, mineral relationships and possible overprinting features.

LA-ICP-MS analysis was carried out using a UP-213 NdYag New Wave pulsed solid state laser, coupled to an Agilent 7500cx ICP Quadrupole Mass Spectrometer (Adelaide Microscopy). Grains of interest within each sample were pre-selected under the SEM to check for compositional inhomogeneity or microinclusions at the grain surface that could influence data quality. Ablation was performed using a consistent spot diameter of 30 μm, a 5 Hz laser pulse rate and 80 % power level. The following isotopes were measured: ^{33}S, ^{34}S, ^{55}Mn, ^{57}Fe, ^{59}Co, ^{60}Ni, ^{65}Cu, ^{66}Zn, ^{69}Ga, ^{75}As, ^{82}Se, ^{95}Mo, ^{107}Ag, ^{111}Cd, ^{115}In, ^{118}Sn, ^{121}Sb, ^{125}Te, ^{197}Au, ^{202}Hg, ^{205}Tl, ^{208}Pb and ^{209}Bi. The total 90 s analysis time included a 30 s background measurement prior to ablation. Calibration was done by using the MASS-1 trace element standard (Wilson et al. 2002). Glitter software (http://www.glitter-gemoc.com/) was used for data reduction. Zinc concentration values, measured by Electron Probe Microanalysis (EPMA) on each sample given the varied Fe contents, were used as internal

standard. Multiple standard analyses were run at the beginning and end of each sequence of 12–15 unknowns to correct for instrument drift.

LA-ICP-MS element maps of a 2×2 mm-sized area of pyrite-sphalerite-chalcopyrite were generated using a Resonetics M-50-LR 193-nm Excimer laser microprobe coupled to an Agilent 7700cx Quadrupole ICP-MS in the same laboratory. Imaging was performed by ablating sets of parallel line rasters across the sample using a 14 μm beam size, line spacing of 14 μm and 28 μm/s scan speed at a laser frequency of 10 Hz and 0.003 s dwell time for all isotopes. Identical rasters were done on reference standard MASS-1 at the start and end of each mapping run to correct for instrument drift. Images were compiled and processed using Iolite (e.g. Woodhead et al. 2007), and Igor, a data analysis program developed by WaveMetrics. Further details of methodology in our laboratory are given in Cook et al. (2013).

Results

Minor and trace element data

Mean concentrations and standard deviations for each element in each sample (total 342 spot analyses) are summarized in Table 2, with inter-element correlations tabulated as Table 3. The full dataset is presented graphically as Fig. 4. A common feature of LA-ICP-MS trace element datasets for sulphides is the high variance for some elements, and the presence of a small number of outliers which impact significantly on the statistical information. This was shown for pyrite by Winderbaum et al. (2012) and is also identified here, with standard deviation exceeding the mean value for some elements in some sub-populations. It is critical to note that although sub-microscopic inclusions are not present at the surface of the analysed micro-volumes, and no direct evidence for them was seen on the time-resolved depth profiles, this does not preclude their presence sub-surface, which might influence data distribution.

The mean concentrations of the two most abundant minor elements in sphalerite (Fe and Cd) are relatively constant across the sample suite (Fig. 4); means for each deposit all lie within the same order of magnitude for both elements.

Manganese shows somewhat greater variation between individual samples than Fe or Cd, with individual concentration values ranging from <30 ppm to >3,000 ppm, even if Mn concentrations within a given sample are relatively constant, as shown by the generally low standard deviations. The unusually high standard deviations relative to means for samples Mo2, STO17504 and 5984B are attributable to a small number of outliers.

Determination of consistent **cadmium** concentrations in each sample (comparable means and relatively low standard deviations; Table 2) is a valuable result. These data are consistent with published work showing that, in sphalerite from metamorphosed massive sulphides, a degree of homogenization is generally present at the sample scale, if not within the deposit as a whole.

Variable concentrations of **cobalt** were determined (Table 2, Fig. 4). The element is present at concentrations of tens to hundreds of ppm in ores from Røros, Sulitjelma and Broken Hill, but is mostly below minimum detection limits (mdl) in samples from Mt. Isa, Mofjellet and Bleikvassli.

Copper concentrations display high variance in samples from Mt Isa, Røros and Sulitjelma. Individual spot analyses for the latter two deposits range from <30 ppm to >10,000 ppm (~1 wt.%). A small number of anomalously high Cu concentrations, due to heterogeneously distributed chalcopyrite disease, significantly skew the sample means. In Bleikvassli, Mofjellet and Broken Hill, mean Cu concentrations are lower and there is also less variation from spot to spot.

Concentrations of **silver** are typically a few ppm in all samples except those from Mt. Isa, where means of 23 and 66 ppm are measured, in both cases with large standard deviations.

The concentration of **gallium** is relatively constant, with means of between 1 and 19 ppm. Measurable and relatively consistent concentrations of **mercury** are determined (less than 300 ppm difference between the lowest and highest mean values). **Thallium** is found to be below or close to mdl in all samples except those from Mt Isa (1–4 ppm).

Lead concentrations vary significantly between different samples from the same deposit and between spots in the same sample. These highly heterogeneous results, coupled with noisy time resolved LA-ICP-MS depth spectra, suggest that Pb occurs mainly as micro- to nanoscale inclusions of galena and/or other Pb-bearing sulphides, significantly skewing the statistical data depending on their density. Particularly high Pb concentrations were measured in spot analyses from sample STO-175-04 (8 out of 18 ablation spots gave Pb concentrations >250 ppm; 3 were >1,000 ppm), and sample V60.446, in which one spot gave 57,458 ppm Pb whereas all other ablation spots for that sample gave <30 ppm. These data indicate that any real lattice-bound Pb is likely to be 'swamped' by the inclusions. Most data points, however, give relatively low Pb, supporting the interpretation (Cook et al. 2009a) that sphalerite is a poor host for lead due to the large ionic size difference between Pb^{2+} and Zn^{2+}, with Pb partitioned into coexisting galena.

Bismuth is noted at mostly <mdl values in samples from Mofjellet, Bleikvassli and Broken Hill, but was >mdl in Mt. Isa, Røros and Sulitjelma. Bismuth ranges up to 500 ppm in one sample from Røros. Many of these high Bi values are from spot analyses which also gave anomalously high Pb and/or Cu, suggesting that many, or possibly all, such higher Bi

Table 2 Summary of LA-ICP-MS data for sphalerite from the analysed samples (data in ppm)

Deposit	Sample		Mn	Fe	Co	Cu	Ga	Ag	Se	Cd	In	Sn	Sb	Hg	Tl	Pb	Bi
Sulitjelma	NC5835 (n=20)	Mean	776	74,406	27	13451[a]	105	6.4	<mdl	1,473	18	4.9	3.5	104	<mdl	3.2	0.18
		S.D	71	42,445	7.5	45,540	9.0	12	–	285	5.3	5.3	5.0	53	–	6.7	0.26
	NC6005 (n=10)	Mean	727	60,213	99	605[a]	2.1	5.9	100	1,786	90	1.8	2.3	38	<mdl	4.4	0.78
		S.D	263	7,179	35	493	2.1	9.0	25	121	21	0.90	2.6	6.4	–	3.7	0.55
	Su-1b (n=20)	Mean	911	81,311	31	574[a]	7.3	4.3	<mdl	1,524	17	<mdl	1.4	44	<mdl	1.0	0.08
		S.D	147	8,708	11	1518[b]	4.7	8.8	–	131	2.2	–	1.4	5.0	–	1.6	0.09
	Su-2a (n=16)	mean	1,275	56,465	27	329	1.3	4.3	71	3,113	5.1	<mdl	1.3	235	<mdl	1.3	0.52
		S.D	201	5,297	4	1261[a]	0.29	4.6	33	293	1.7	–	1.6	48	–	1.8	0.98
	Su-2b (n=20)	Mean	1,351	72,921	31	67	1.5	3.4	37	2,873	5.3	<mdl	1.0	178	<mdl	3.3	1.2
		S.D	190	10,483	7.0	151	0.70	2.4	15	257	1.4	–	0.99	25	–	5.4	4.5
Mofjell	Mo2 (n=18)	Mean	589	32,142	<mdl	9.1	1.2	1.0	<mdl	2,012	1.7	<mdl	<mdl	173	<mdl	22	<mdl
		S.D	216	3,671	–	6.8	2.1	0.53	–	138	0.07	–	–	99	–	72	–
	Mo5 (n=20)	Mean	1,446	59,561	<mdl	8.0	1.8	1.4	<mdl	2,110	2.3	<mdl	<mdl	212	<mdl	1.2	<mdl
		S.D	314	2,709	–	3.0	0.43	1.1	–	115	0.16	–	–	60	–	0.95	–
	Mo10 (n=20)	Mean	957	43,640	<mdl	6.5	1.3	0.97	<mdl	1,988	1.2	<mdl	<mdl	290	<mdl	2.1	<mdl
		S.D	46	3,818	–	2.1	0.46	0.12	–	103	0.07	–	–	88	–	4.3	–
Røros	STO17504 (n=18)	Mean	469	74,576	226	12619[b]	1.3	11	91	1,310	40	3.0	0.26	39	0.10	440[b]	69[b]
		S.D	584	35,700	24	40,508	1.6	11	25	71	11	4.1	0.29	9.8	0.14	676	143
	STO17505 (n=20)	Mean	492	57,768	32	457[b]	1.3	4.1	121	1,187	28	0.60	0.83	41	<mdl	29	3.2
		S.D	68	2,661	2.0	1,418	0.45	2.9	31	37	2.3	0.62	1.0	3.7	–	61	2.9
	STO17506 (n=20)	Mean	1,135	64,579	127	40	5.6	1.7	47	1,139	8.3	0.80	0.43	25	<mdl	2.9	2.0
		S.D	30	1,048	9.9	39	1.1	1.8	6.6	15	0.16	0.24	0.7	3.3	–	5.2	3.2
Bleikvassli	Bv1 (n=20)	Mean	313	62,698	<mdl	76	19	2.6	<mdl	1,405	56	5.1	1.3	135	<mdl	24	<mdl
		S.D	104	3,250	–	29	1.4	2.7	–	75	3.0	9.4	2.5	26	–	61	–
	V59.197 (n=20)	Mean	758	72,318	<mdl	115	6.0	2.1	<mdl	1,273	119	<mdl	0.76	155	0.01	2.6	0.01
		S.D	78	5,187	–	7.2	0.88	1.1	–	27	4.0	–	1.0	29	0.03	6.6	–
	V60.446 (n=20)	Mean	2,751	54,962	<mdl	75	1.9	5.3	<mdl	1,458	87	2.5	3.7	108	<mdl	2695[b]	<mdl
		S.D	197	4,259	–	17	0.39	13	–	74	18	3.3	6.8	21	–	12,857	–
	V61.538 (n=20)	mean	2,079	63,772	<mdl	47	5.8	1.3	<mdl	1,560	52	5.0	0.63	68	<mdl	0.37	<mdl
		S.D	245	4,376	–	4.9	0.34	0.50	–	48	1.5	3.9	1.4	5.2	–	0.59	–
Mt. Isa	5984A (n=20)	Mean	55	45,779	<mdl	121[a]	<mdl	23	<mdl	1,879	8.9	<mdl	26	113	1.3	12041[b]	0.35
		S.D	15	2,499	–	196	–	24	–	90	4.5	–	34	29	2.1	41,651	1.2
	5984B (n=20)	Mean	297	47,790	<mdl	63[a]	0.45	66	<mdl	1,967	25	<mdl	86	65	3.4	56005[b]	1.4
		S.D	585	28,192	–	102	0.30	172	–	204	8.6	–	229	32	8.8	169,040	4.3
Broken Hill	BH218 (n=20)	Mean	1,705	74,090	62	34	6.7	1.9	<mdl	1,667	2.9	<mdl	0.11	21	<mdl	1.9	<mdl
		S.D	93	2,170	7.8	7.7	0.27	1.5	–	86	0.16	–	0.09	5.8	–	2.5	–
	BH221 (n=20)	Mean	775	59,203	93	28	4.7	4.0	<mdl	2,824	2.6	<mdl	0.26	41	<mdl	2.7	<mdl
		S.D	67	8,980	9.3	7.5	0.47	2.9	–	142	0.17	–	0.31	21	–	3.8	–

Typical mdl values: Co 0.4 ppm; Ga 0.25 ppm; Se 20–30 ppm; Sn 0.3 ppm; Sb 0.3 ppm; Tl; 0.05 ppm; Bi 0.05 ppm

[a] Chalcopyrite disease

[b] Sub-micron-scale inclusions

concentrations result from inclusions of Cu-Pb-Bi sulphosalts. In other samples from Sulitjelma and Røros, Bi was found to be <10 ppm.

Antimony is mostly present at concentrations >mdl (up to 16 ppm), except in samples from Mofjellet (consistently <mdl) and Mt. Isa (higher mean concentrations heavily influenced by a small number of outliers). Most analysed spot values were between 0.1 and 4 ppm. **Selenium** is present at concentrations >mdl only in the Røros and some Sulitjelma samples. It should be noted, however, that mdl values for Se (20–30 ppm) are significantly higher than for most other elements. Concentrations of **indium** lie above mdl values in

Table 3 Inter-element correlations (r′ values)

	Mn	Fe	Co	Cu	Ga	As	Se	Ag	Cd	In	Sn	Sb	Te	Hg	Pb
Fe	0.285														
Co	−0.046	0.426													
Cu	−0.177	0.340	0.133												
Ga	0.298	**0.617**	0.104	0.220											
As	−0.146	0.226	0.010	−0.106	0.069										
Se	−0.382	−0.171	0.367	−0.159	−0.208	0.027									
Ag	−0.332	0.014	0.196	0.469	−0.256	0.121	0.056								
Cd	0.128	−0.279	−0.097	−0.501	−0.365	0.311	0.105	0.019							
In	−0.109	0.250	−0.136	**0.745**	0.242	−0.246	0.251	0.270	**−0.608**						
Sn	0.158	0.208	−0.009	0.458	0.297	−0.191	0.092	0.247	−0.128	0.436					
Sb	−0.236	−0.159	−0.145	0.316	−0.234	0.123	0.206	**0.710**	0.033	0.246	0.212				
Te	−0.003	0.005	−0.134	−0.101	0.221	0.125	0.063	−0.414	−0.071	−0.059	−0.064	0.176			
Hg	0.076	−0.286	−0.533	−0.294	−0.179	0.434	0.067	0.220	0.433	−0.199	−0.205	0.064	0.493		
Pb	−0.416	−0.321	0.175	0.102	−0.469	−0.098	0.211	**0.662**	0.031	−0.039	0.004	0.567	−0.191	−0.192	
Bi	−0.134	0.007	0.341	0.153	−0.256	−0.215	0.398	0.249	0.160	−0.066	0.131	0.274	0.180	−0.084	0.374

Numbers in bold show particularly strong correlations (>0.5 or <-0.5)

all samples. Sphalerite from Sulitjelma, Bleikvassli and Røros is enriched in the element (means of tens of ppm). **Tin** concentrations are <mdl in the Mt Isa, Mofjellet and Broken Hill samples. Measurable Sn, up to a few ppm, was determined in some of the Sulitjelma, Bleikvassli and Røros samples.

Element maps

Insights into element partitioning among co-existing sulphides can be gained from LA-ICP-MS element maps of a sphalerite-chalcopyrite assemblage from Sulitjelma (Fig. 5). Cadmium, Mn, Hg and In are preferentially incorporated into sphalerite. Indium and Mn are also present in chalcopyrite but at significantly lower concentrations. Although Ga mimics this behaviour (sph>cpy>py), Ge does not; this element is present in pyrite at concentrations above those in the base metal sulphides. In this sample, Co, Ni and As are preferentially enriched in pyrite, with maps for Co and Ni showing evidence of relict compositional zoning. Sphalerite is shown to be a relatively poor host for Co, albeit at concentrations higher than in coexisting chalcopyrite. Silver and Sn are enriched in chalcopyrite relative to other sulphides but sphalerite contains greater concentrations of both elements than pyrite.

Discussion

Although several studies have applied LA-ICP-MS techniques to analysis of sphalerite (Axelsson and Rodushkin 2001; Cook et al. 2009a, 2011; Ye et al. 2011), uncertainties persist about the real range of minor and trace element concentrations. This is due, in part, to the difficulty of discriminating between elements hosted within the sphalerite crystal lattice and elements hosted within nano- to submicron-scale inclusions. The latter are generally only visible using high-resolution imaging (e.g. Ciobanu et al. 2011) but time-resolved LA-ICP-MS depth profiles can offer indirect information regarding the presence of sub-micron-scale inclusions. They cannot, however, differentiate between lattice-bound trace elements and nanoparticles if the latter are homogeneously distributed throughout the sampled volume.

Syn-metamorphic recrystallization of sphalerite

The broad effects of metamorphism and associated deformation on sulphide ores have been summarized in a number of publications (Vokes 1969; Mookherjee 1970; Craig and Vokes 1993; Spry et al. 2000). The effects of metamorphism on the distributions of minor and trace element distributions are however less well constrained and there are relatively few published data for sulphides other than pyrite. The six deposits studied here (Table 1) are all regionally metamorphosed, at facies conditions ranging from greenschist facies through lower and upper amphibolite facies up to granulite facies, thus facilitating discussion of the effects of metamorphism on trace element distributions of sphalerite.

Application of the Fe content of sphalerite as a geobarometer is well established. Sphalerite-pyrite-pyrrhotite equilibrium will result in sphalerite becoming progressively less Fe-rich with increasing pressure (Scott and Barnes 1971; Scott 1973). No observable trend between Fe and metamorphic grade in seen the sample suite analysed here. This is most likely due to the lack of equilibrium crystallization of

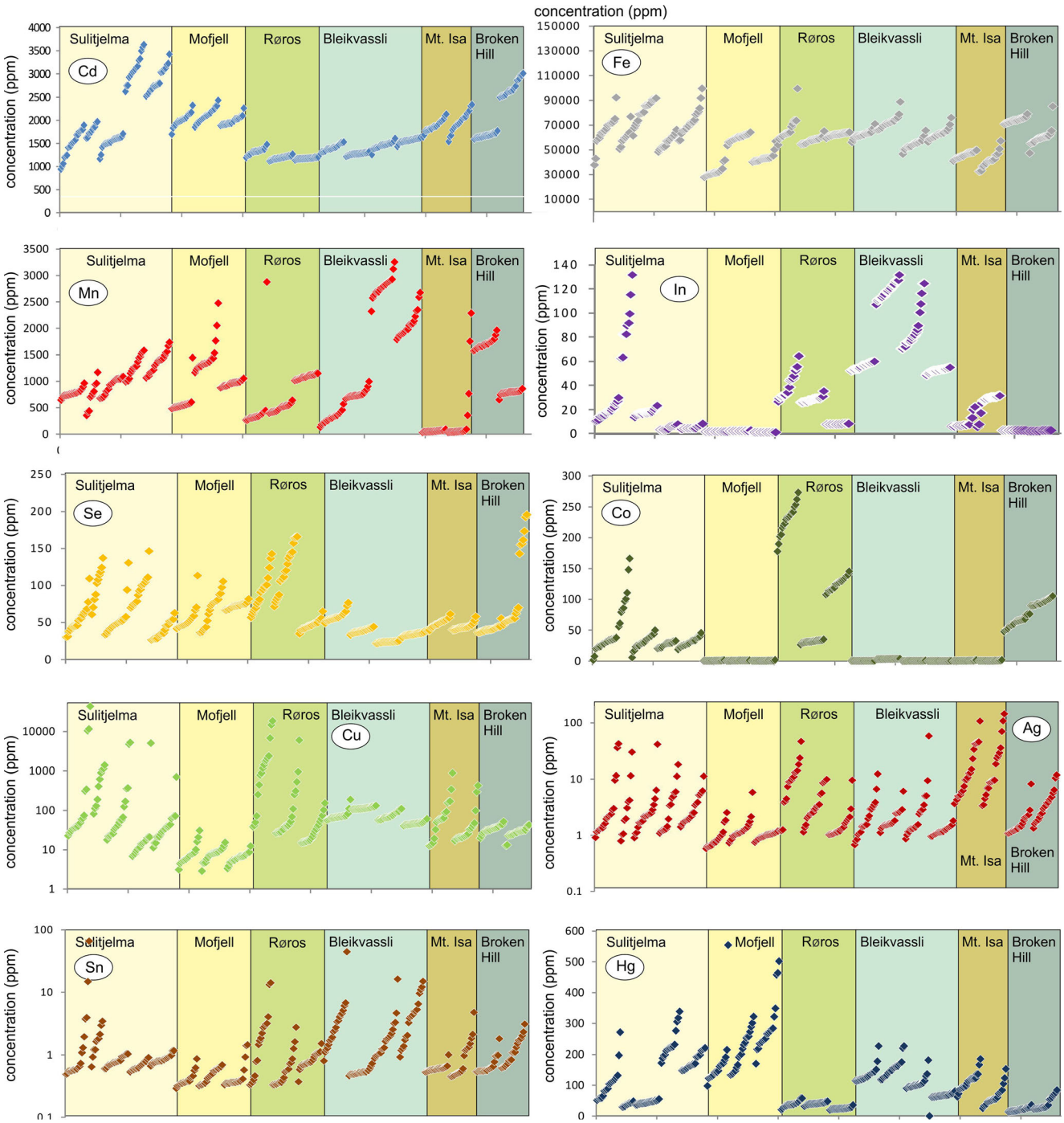

Fig. 4 Graphical representations of element abundances (in ppm) of Cd, Fe, Mn, In, Se, Co, Cu, Ag, Sn and Hg plotted as a cumulative plot. Cu, Ag and Sn are plotted on a logarithmic scale. The concentrations in individual samples from the different deposits are arranged on the *horizontal axis*. The reader is referred to Table 2 for numerical data and statistical treatment. Data plotted are considered to represent element concentrations in sphalerite crystallized under equilibrium at peak metamorphic conditions

sphalerite with both pyrite and pyrrhotite (Cook et al. 1994). Cobalt concentrations in sphalerite also show little correlation with metamorphic grade.

The effect of metamorphic grade on the Cu concentration is quite clear. Sphalerite in samples from the three upper amphibolite or granulite facies deposits (Mofjellet, Bleikvassli and Broken Hill) show significantly greater homogeneity in their Cu concentrations, even in the presence of co-existing chalcopyrite. The lower grade deposits showed higher mean Cu concentrations overall, but the influence of very high individual values is marked. Without the impact of chalcopyrite disease, average Cu concentrations for the deposits are

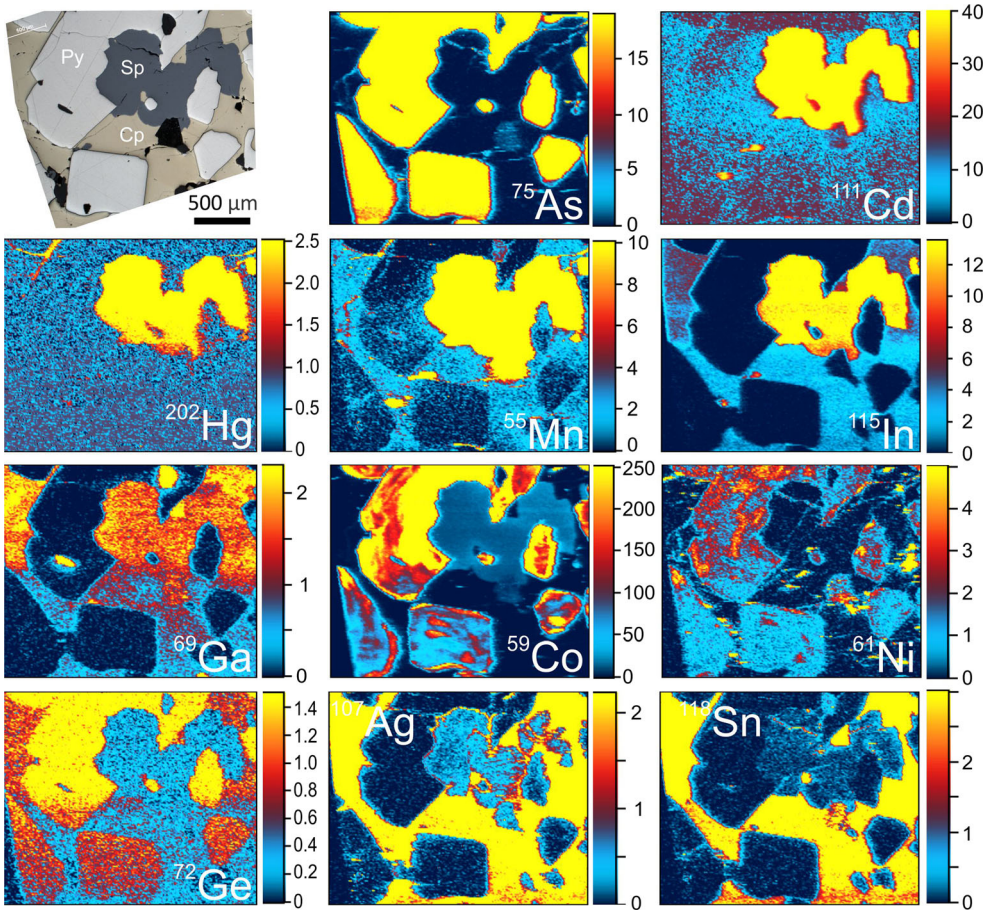

Fig. 5 Reflected light photomicrograph (*top left*) and LA-ICP-MS element maps for selected elements in a sphalerite-chalcopyrite-pyrite assemblage (Sulitjelma). Scales are in counts-per-second ($\times 10^3$)

generally within a single order of magnitude. Sphalerite in those deposits which experience recrystallization at upper amphibolite or granulite facies conditions contains little to no chalcopyrite disease. A model for development of chalcopyrite disease (Barton and Bethke 1987) involves replacement of high-Fe sphalerite by an aggregate of chalcopyrite and low-Fe sphalerite takes place during cooling. If chalcopyrite disease is thus considered to be a retrograde phenomenon, it should be equally abundant in all deposits. A logical explanation is that chalcopyrite excretions in sphalerite are released and then remobilized during recrystallization at highest metamorphic conditions.

Concentrations of Mn, and to some degree also Ga, show a possible weak relationship with metamorphic grade (Table 2), even if there is also considerable variation among individual samples from any given deposit. Concentration ranges are consistent with published values in VHMS deposits (Cook et al. 2009a and references therein). Although mean values for Ag, Cd and In show distinctive differences in range between the six deposits, no consistent trend in relation to metamorphic grade can be observed in the results. Cook et al. (2009a) considered that In enrichment in sphalerite is linked to source rocks and the partitioning of the element among co-existing minerals. Mercury concentrations are highest in sphalerite from Sulitjelma, Mofjellet and Bleikvassli. We interpret this trend in terms of Hg being readily re-incorporated into sphalerite during recrystallization. The lack of Hg in sphalerite from Broken Hill may be linked to its substitution instead in co-existing galena.

Bismuth is present at concentrations mostly above mdl in sphalerite from Mt Isa, Røros and Sulitjelma, whereas it is consistently <mdl in the upper amphibolite to granulite facies deposits. This suggests a possible link between metamorphic grade and Bi concentrations in sphalerite. Bismuth is, however, not considered to partition into sphalerite particularly well (Cook et al. 2009a) and, among these higher concentrations, variance is typically high. This heterogeneity indicates that bismuth may exist as micro-inclusions in sphalerite and as such, complete crystallization of sphalerite (Bleikvassli, Mofjell and Broken Hill) simply purges the sphalerite of many of the smaller inclusions. A further argument is the abundance of galena in these; Bi is partitioned into that mineral (i.e., George L, Cook NJ, Ciobanu CL (accepted) Trace and minor elements in galena: a reconnaissance LA-ICP-MS study. Am Mineral). Lastly, primary metal source may also play a role. Certainly, some sulphide bodies in both the Røros and Sulitjelma districts are moderately enriched in Bi, with discrete Bi-minerals observed in ore remobilizates in both deposits (Cook, unpubl. data). Discrete Bi-minerals are not

known from Bleikvassli (Cook et al. 1998) and are scarce at Broken Hill.

Minor and trace element abundances

The consistent Cd concentrations in each sample (similar means and relatively low standard deviations, Table 2), are in agreement with published work showing that in stratiform ores Cd tends to on average range from 0.1 to 1.5 wt.%. In both MVT deposits and Zn-rich veins in carbonate rocks, Cd can occur at higher concentrations in sphalerite, which can be an important source for by-product Cd (Schwartz 2000; Ye et al. 2012).

The Co ion is similar in size to that of Fe (Cook et al. 2009a) and as such can be expected to be substituted within sphalerite in moderate amounts. Differences in Co concentrations between deposits in which Co is present at concentrations of tens to hundreds of ppm (Røros, Sulitjelma and Broken Hill) and those where the element is <mdl (Mt. Isa, Mofjellet and Bleikvassli) possibly indicates that Co incorporation is limited by its availability in the leached source rock and, implicitly, genetic type. Volcanic rocks could be the Co source in the two VHMS deposits but also for Broken Hill, which although classed as a SEDEX-type deposit, is noted to contain significant volcanic influences (Haydon and McConachy 1987). The presence or absence of pyrite, a god Co host, may also influence Co concentrations in sphalerite.

In the absence of a trivalent ion facilitating coupled substitution, Cu is not widely considered to be readily incorporated into the sphalerite lattice and is more commonly observed as tiny 'excretions' of chalcopyrite (chalcopyrite disease). Variations in Cu concentration are thus mostly due to variation in the density of chalcopyrite inclusions in sphalerite rather than real lattice-bound Cu. The greater homogeneity of Cu concentrations in sphalerite from the Bleikvassli, Mofjellet and Broken Hill deposits is consistent with the lack of chalcopyrite disease. Coupled with flat Cu signals on the time-resolved LA-ICP-MS depth profiles in these samples, this infers that Cu can be substituted, at low concentrations, within the sphalerite lattice.

Gallium occurs in solid solution in sphalerite at up to 20 mol% Ga_2S_3 (Kramer et al. 1987) and has been reported to occur at high concentrations in sphalerite from some carbonate-hosted and MVT deposits.

The Mt Isa samples show strong Ag enrichment in sphalerite and contrasts with the Broken Hill samples where sphalerite is Ag-poor. This indicates that, in lower-temperature deposits such as SEDEX, sphalerite is likely to be an important Ag carrier but such Ag will be remobilised to form discrete Ag minerals during metamorphism.

Variation in the In concentration between different samples is greater than that of Ga or Ag, but the element nevertheless demonstrates homogeneity between ablation spots in the same sample (low standard deviations, Table 2). Indium is generally considered to be incorporated within sphalerite via the coupled substitution $2Zn^{2+} \leftrightarrow Cu^{+} + In^{3+}$.

The relatively consistent Hg concentrations, and generally low standard deviations relative to the means, indicate that Hg is most likely lattice-bound ($Zn^{2+} \leftrightarrow Hg^{2+}$).

Inter-element relationships

One goal of our study was to identify any relationships among the elements analysed. Although there are few strong correlations between element pairs (Table 3) some inter-element relationships carry petrogenetic value. Positive correlations are noted between In and Cu (Fig. 6a), Ag and Cu (Fig. 6b), Ag and Pb (Fig. 6c), and Ag and Sb (Fig. 6d). Abundant chalcopyrite disease in some samples masks the otherwise strong correlation between In and Cu (Fig. 6a). Previous studies of sphalerite (Cook et al. 2009a, 2011, 2012) have supported the coupled substitution $2Zn^{2+} \leftrightarrow Cu^{+} + In^{3+}$ for In substitution in the sphalerite lattice. This study shows that sphalerite from Mt. Isa, Røros, Sulitjelma and Bleikvassli are enriched in indium; this was not known at the time these deposits were under exploitation.

Cook et al. (2009a), Ciobanu et al. (2011) and Murakami and Ishihara (2013) found that Ag can exist as microscopic Ag-bearing mineral inclusions in sphalerite as well as substituted in the lattice (as Ag^{+}). Correlations between Ag and Cu, Pb and Sb (Fig. 6b–d, respectively) may reflect this dual character. It is easy to attribute higher Ag concentrations, particularly when Pb is also high, to small inclusions of discrete minerals, yet the strong correlation between Ag and Sb can also be explained by coupled substitution in the sphalerite lattice: $2Zn^{2+} \leftrightarrow Cu^{+} + Sb^{3+}$.

There is scant evidence for correlation among Mn, Fe and Cd. Mn/Fe ratios also show no obvious trend across the dataset. Di Benedetto et al. (2005), focussing on compositionally-zoned sphalerite, indicated that Mn and Fe compete in substituting for Zn in sphalerite, creating regions that are relatively high in one and low in the other which should result in a negative correlation between the two elements. Figure 6e shows the negative correlation between Co and Hg. Co-enrichment in sphalerite is seen in those deposits hosted by Co-rich mafic volcanic rocks (VHMS-type) whereas Hg is higher in those hosted within sequences dominated by sedimentary rocks (SEDEX-type). The comparable relationship between Cd and In (Fig. 6f) may possibly reflect an analogous control by host rock lithology, even if the plot also shows significant variation of the Cd/In ratio within individual deposits, particularly Sulitjelma.

In their study of trace element signatures of sphalerite in different genetic types of deposit within a restricted geographic area in southern China, Ye et al. (2011) found that the signature of SEDEX- and VHMS-type deposits (non- or

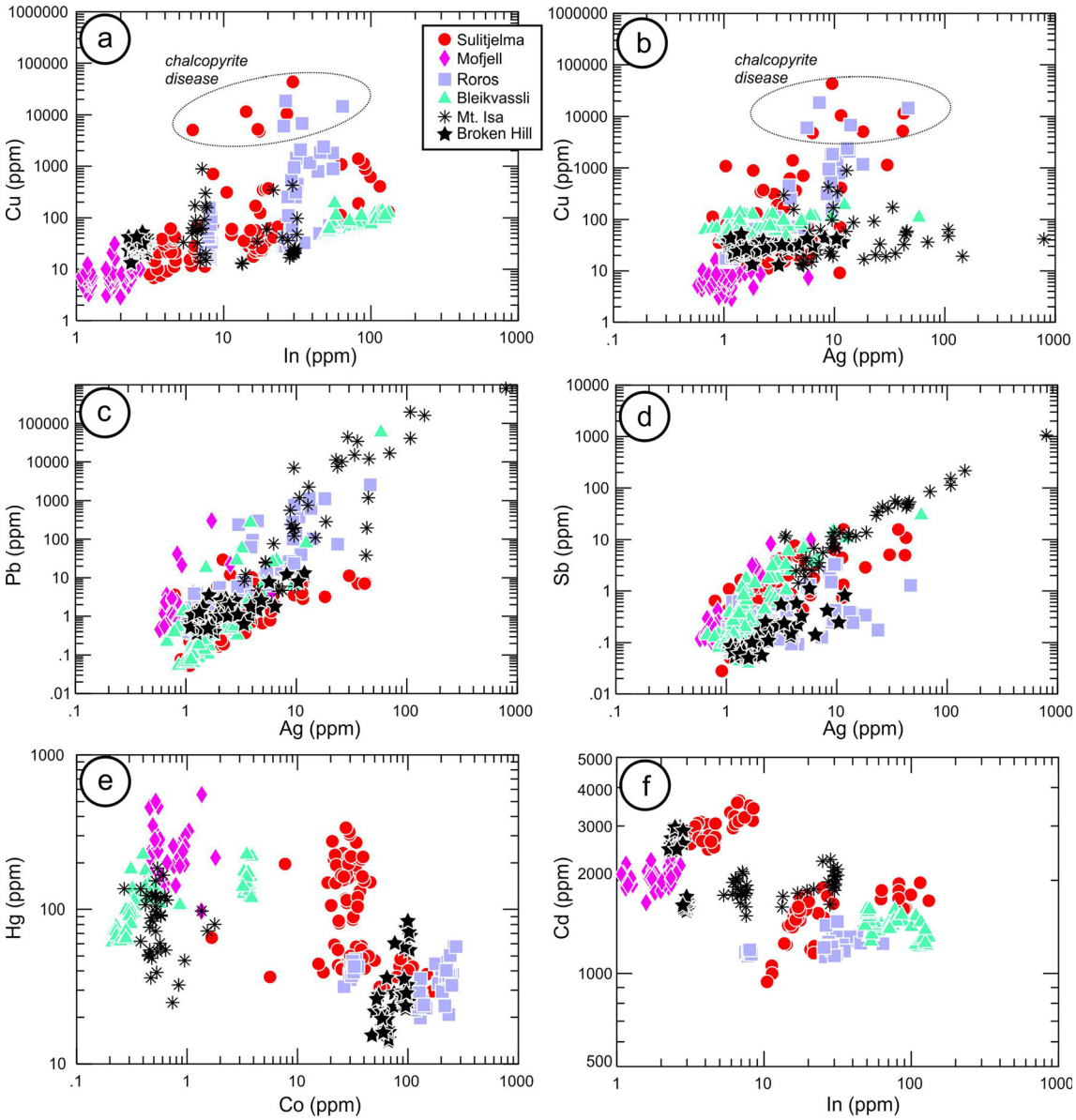

Fig. 6 Binary element plots. **a** In vs. Cu; **b** Ag vs. Cu; **c** Ag vs. Pb; **d** Ag vs. Sb; **e** Hg vs. Co; and **f** Cd vs. In. Note how data from some samples from the same deposit (e.g. Røros) cluster together, whereas data from others, notably Sulitjelma, is more spread out on each plot

weakly metamorphosed) are distinct from those of skarns and MVT deposits. Differences among SEDEX- and VHMS-type deposits can be correlated with the leached source rocks, notably relative proportions of sediments and mafic volcanic rocks.

Concluding remarks

Although there is little evidence for any systematic relationships between conditions of regional metamorphism and trace element concentrations in sphalerite, some elements, notably Cu, are lower and more homogeneously distributed in recrystallized sphalerite. Other elements (Pb, Bi, Ag, possibly Sn and Sb) are released during recrystallization; others (Fe, Cd, Mn, In) are readily re-incorporated. No compositional zoning was observed in recrystallized sphalerite. Absolute element concentration ranges are, however, strongly influenced by the relative abundance of the elements in the pre-metamorphic mineral, which are in turn is controlled by the physical-chemical parameters at the time of initial crystallization, source of ore-forming fluids and element partitioning between sphalerite and co-existing sulphides.

Some of these interpretations demand additional confirmation through study of a wider sample suite. One line of enquiry would be to examine metamorphosed examples of other types

of sphalerite-bearing deposits, particularly MVT and skarn-related sphalerite.

Ore petrologists have long sought to obtain temperatures of mineral equilibration using the distribution of trace elements between two coexisting phases. Given that sphalerite accommodates a variety of trace elements, sphalerite has considerable potential as a geothermometer. Indeed, trace element geothermometers based on the partitioning of Cd, Mn and Se between coexisting sphalerite and galena were proposed more than 40 years ago based on experimentally determined distribution constants (Bethke and Barton 1971). Given the accuracy and sensitivity of modern microanalytical techniques, quantification of element partitioning between sphalerite and coexisting minerals (galena, chalcopyrite etc.) should be possible in samples for which the crystallization temperature can be independently constrained. Encouragement for this is seen in a reconnaissance study of trace element concentrations in galena from base metal ores (George et al. accepted), including some deposits from which sphalerite was analyzed here.

Acknowledgments We gratefully thank Angus Netting and Benjamin Wade (Adelaide Microscopy) for assistance with analytical work. The comments of Reiner Klemd, an anonymous reviewer, and Associate Editor Anton Beran greatly assisted us with clarifying our ideas. This is TRaX contribution 295.

References

Axelsson MD, Rodushkin I (2001) Determination of major and trace elements in sphalerite using laser ablation double focusing sector field ICP-MS. J Geochem Explor 72:81–89

Barrie CD, Boyce AJ, Boyle AP, Williams PJ, Blake K, Wilkinson JJ, Lowther M, McDermott P, Prior DJ (2009) On the growth of colloform textures: a case study of sphalerite from the Galmoy ore body, Ireland. J Geol Soc Lond 166:563–582

Barrie CD, Cook NJ, Boyle AP (2010a) Textural variation in the pyrite-rich ore deposits of the Røros district, Trondheim Region, Norway: implications for pyrite deformation mechanisms. Mineral Deposita 45:51–68

Barrie CD, Boyle AP, Cook NJ, Prior DJ (2010b) Pyrite deformation textures in the massive sulfide ore deposits of the Norwegian Caledonides. Tectonophysics 483:269–286

Barton PB, Bethke PM (1987) Chalcopyrite disease in sphalerite—pathology and epidemiology. Am Mineral 72:451–467

Beaudoin G (2000) Acicular sphalerite enriched in Ag, Sb, and Cu embedded within colour banded sphalerite from the Kokanee Range, BC. Can Mineral 38:1387–1398

Bell TH, Hickey KA (1998) Multiple deformations with successive subvertical and subhorizontal axial planes in the Mount Isa region, their impact on geometric development and significance for mineralization and exploration. Econ Geol 96:1369–1389

Bethke PM, Barton PB (1971) Sub-solidus relations in the system PbS-CdS. Am Mineral 56:2034–2039

Bjerkgård T, Larsen RB, Marker M (1995) Regional geology of the Okstindene area, the Rødingsfjäll Nappe Complex, Nordland, Norway. Open Rep, Nor Geol Unders 95.153: 87 pp

Bjerkgård T, Sandstad JS, Sturt BA (1999) Massive sulphide deposits in the South-Eastern Trondheim Region Caledonides, Norway: a review. In: Stanley CJ et al (eds) Mineral deposits: processes to processing: Proceedings of the Fifth Biennial SGA Meeting. A.A. Balkema, p 935–938

Bjerkgård T, Marker M, Sandstad JS, Cook NJ, Sordahl T (2001) Ore potential with emphasis on gold in the Mofjellet deposit, Rana, Nordland, Norway. Norges geol unders report 2001.050

Both RA, Rutland RWR (1976) The problem of identifying and interpreting stratiform ore bodies in highly metamorphosed terrains: the Broken Hill example. In: Wolf KH (ed) Handbook of stratabound and stratiform ore deposits, 4. Elsevier, Amsterdam, pp 261–325

Boyle AP, Westhead RK (1992) Metamorphic peak geothermobarometry in the Furulund Group, Sulitjelma, Scandinavian caledonides—implications for uplift. J Metamorph Geol 10:615–626

Bugge JAW (1978) Norway. In: Bowie SHU, Kvalheim A, Haslam HW (eds) Mineral deposits of Europe, vol 1, North-west Europe. IMM/Min Soc, London, pp 199–249

Ciobanu CL, Cook NJ, Utsunomiya S, Pring A, Green L (2011) Focussed ion beam-transmission electron microscopy applications in ore mineralogy: bridging micro- and nanoscale observations. Ore Geol Rev 42:6–31

Ciobanu CL, Cook NJ, Utsunomiya S, Kogagwa M, Green L, Gilbert S, Wade B (2012) Gold-telluride nanoparticles revealed in arsenic-free pyrite. Am Mineral 97:1515–1518

Cook NJ (1992) Antimony-rich mineral parageneses and their association with Au minerals within massive sulphide deposits at Sulitjelma, Norway. N Jb Mineral Monatsh 97–106

Cook NJ (1993) Conditions of metamorphism estimated from alteration lithologies and ore at the Bleikvassli Zn–Pb–(Cu) deposit, Nordland, Norway. Nor Geol Tidsskr 73:226–233

Cook NJ (1994) Post-recrystallisation phenomena in metamorphosed stratabound sulphide ores: a comment. Mineral Mag 58:480–484

Cook NJ (1996) Mineralogy of the sulphide deposits at Sulitjelma, northern Norway. Ore Geol Rev 11:303–338

Cook NJ (2001) Ore mineralogical investigation of the Mofjell deposit (Mo i Rana, Nordland, Norway) with emphasis on gold and silver distribution. Norges geol unders Report 2001.051: 31 pp

Cook NJ, Hoefs J (1997) Sulphur isotope characteristics of metamorphosed Cu-(Zn) volcanogenic massive sulphide deposits in the Norwegian Caledonides. Chem Geol 135:307–324

Cook NJ, Halls C, Kaspersen PO (1990) The geology of the Sulitjelma ore field, northern Norway—some new interpretations. Econ Geol 85:1720–1737

Cook NJ, Halls C, Boyle AP (1993) Deformation and metamorphism of massive sulphides at Sulitjelma, Norway. Mineral Mag 57:67–81

Cook NJ, Klemd R, Okrusch M (1994) Sulphide mineralogy, metamorphism and deformation in the Matchless massive sulphide deposit, Namibia. Mineral Deposita 29:1–15

Cook NJ, Spry PG, Vokes FM (1998) Mineralogy and textural relationships among sulphosalts and related minerals in the Bleikvassli Zn-Pb-(Cu) deposit, Nordland, Norway. Mineral Deposita 34:35–56

Cook NJ, Ciobanu CL, Pring A, Skinner W, Shimizu M, Danyushevsky L, Saini- Eidukat B, Melcher F (2009a) Trace and minor elements in sphalerite: a LA-ICPMS study. Geochim Cosmochim Acta 73: 4761–4791

Cook NJ, Ciobanu CL, Mao JW (2009b) Textural control on gold distribution in As-free pyrite from the Dongping, Huangtuliang and Hougou gold deposits, North China Craton, (Hebei Province, China). Chem Geol 264:101–121

Cook NJ, Sundblad K, Valkama M, Nygård R, Ciobanu CL, Danyushevsky L (2011) Indium mineralisation in A-type granites in southeastern Finland. Chem Geol 284:62–73

Cook NJ, Ciobanu CL, Brugger J, Etschmann B, Howard DL, de Jonge MD, Ryan C, Paterson D (2012) Determination of the oxidation

state of Cu in substituted Cu-In-Fe-bearing sphalerite via μ-XANES spectroscopy. Am Mineral 97:476–479

Cook NJ, Ciobanu CL, Meria D, Silcock D, Wade B (2013) Arsenopyrite-pyrite association in an orogenic gold ore: tracing mineralization history from textures and trace elements. Econ Geol 108:1273–1283

Craig JR, Vokes FM (1992) Ore mineralogy of the Appalachian–Caledonian stratabound sulfide deposits. Ore Geol Rev 7:77–123

Craig JR, Vokes FM (1993) The metamorphism of pyrite and pyritic ores—an overview. Mineral Mag 57:3–18

Danyushevsky L, Robinson P, Gilbert S, Norman M, Large R, McGoldrick P, Shelley M (2011) Routine quantitative multi-element analysis of sulphide minerals by laser ablation ICP-MS: standard development and consideration of matrix effects. Geochem Explor Environ Anal 11:51–60

Deol S, Deb M, Large RR, Gilbert S (2012) LA-ICPMS and EPMA studies of pyrite, arsenopyrite and loellingite from the Bhukia-Jagpura gold prospect, southern Rajasthan, India: implications for ore genesis and gold remobilization. Chem Geol 326–327:72–87

Di Benedetto F, Bernardini GP, Costagliola P, Plant D, Vaughan DJ (2005) Compositional zoning in sphalerite crystals. Am Mineral 90:1384–1392

Finlow-Bates T, Stumpfl EF (1985) Lead isotope studies bearing on the genesis of copper orebodies at Mount Isa, Queensland and Mount Isa silica dolomite and copper orebodies, the result of syntectonic hydrothermal alteration system—a discussion. Econ Geol 80:186–188

Frost BR, Mavrogenes JA, Tomkins AG (2002) Partial melting of sulfide ore deposits during medium- and high-grade metamorphism. Can Mineral 40:1–18

Frost BR, Swapp SM, Gregory RW (2005) Prolonged existence of sulfide melt in the Broken Hill orebody, New South Wales, Australia. Can Mineral 43:479–493

Fryer BJ, Jackson SE, Longerich HP (1995) Design, operation and role of the Laser-Ablation Microprobe coupled with an Inductively-Coupled Plasma - Mass-Spectrometer (LAM-ICP-MS) in the earth-sciences. Can Mineral 33:303–312

Gee DG, Sturt BA (1985) The Caledonide orogen: Scandinavia and related areas. Wiley, New York

Genkin AD, Bortnikov NS, Cabri LJ, Wagner FE, Stanley CJ, Safonov YG, McMahon G, Friedl J, Kerzin AL, Gamyanin GM (1998) A multidisciplinany study of invisible gold in arsenopyrite from four mesothermal gold deposits in Siberia, Russian Federation. Econ Geol 93:463–487

Greenfield JE, Lees TC, Parr JM, McConachy TF (2003) A review of Broken Hill ore system models. Geosci Aust Rec 2003(13): 57–60

Grenne T, Ihlen PM, Vokes FM (1999) Scandinavian Caledonide Metallogeny in a plate tectonic perspective. Mineral Deposita 34: 422–471

Grondijis HF, Schouten C (1937) A study of the Mt. Isa ores. Econ Geol 32:407–450

Haydon RC, McConachy GW (1987) The stratigraphic setting of Pb-Zn-Ag mineralization at Broken Hill. Econ Geol 82:826–856

Ihlen PM, Grenne T, Vokes FM (1997) Metallogenic evolution of the Scandinavian Caledonides. Trans Inst Min Metall 106:194–203

Knight CL (1953) Regional geology of Mount Isa. 5th Empire Mining Metall. Congr, Melbourne, Publ 1, p 352–360

Kramer V, Hirth H, Hofherr W, Trah HP (1987) Phase studies in the systems Ag_2Te-Ga_2Te_3, ZnSe-In_2Se_3, and ZnS-Ga_2S_3. Thermochim Acta 112:89–94

Laing WP, Marjoribanks RW, Rutland RWR (1978) Structure of the Broken Hill mine area and its significance for the genesis of the ore bodies. Econ Geol 73:1112–1136

Large RR, Bull SW, McGoldrick PJ, Walters S, Derrick GF, Carr GR (2005) Stratiform and Strata-Bound Zn-Pb-Ag Deposits in Proterozoic Sedimentary Basins, Northern Australia. Econ Geol 100th Anniv Vol 931–963

Large RR, Danyushevsky L, Hollit C, Maslennikov V, Meffre S, Gilbert S, Bull S, Scott R, Emsbo P, Thomas H, Singh B, Foster J (2009) Gold and trace element zonation in pyrite using a laser imaging technique: implications for the timing of gold in orogenic and Carlin-style sediment-hosted deposits. Econ Geol 104:635–668

Larocque ACL, Hodgson CJ, Cabri LJ, Jackman JA (1995) Ion microprobe analysis of pyrite, chalcopyrite and pyrrhotite from the Mobrun VMS deposit in Northwestern Quebec: evidence for metamorphic remobilization of gold. Can Mineral 33:373–388

Lawrence LJ (1967) Sulphide neomagmas and highly metamorphosed sulphide deposits. Mineral Deposita 2:5–10

Mathias BV, Clark GJ (1975) Mount Isa copper and silver-lead-zinc orebodies. Isa and Hilton mines. In: Knight CL (ed) Economic geology of Australia and Papua New Guinea. I. Metals. AusIMM Monogr 5, p 351–372

Mavrogenes JA, MacIntosh IW, Ellis DJ (2001) Partial melting of the Broken Hill galena–sphalerite ore; experimental studies in the system PbS–Fe–S–Zn–S–(Ag_2S). Econ Geol 96:205–210

McClay KR (1979) Folding in silver-lead-zinc orebodies, Mount Isa, Australia. Trans Inst Min Metall 88:B5–B14

McGoldrick PJ, Keays RR (1990) Mount Isa copper and lead-zinc-silver deposits: coincidence or cogenesis? Econ Geol 85:641–651

Mookherjee A (1970) Dykes, sulphide deposits, and regional metamorphism—criteria for determining their time relationship. Mineral Deposita 5:120–144

Moralev GV, Larsen RB, Bjerkgård T (1995) Distribution of precious metals in the Bleikvassli Zn-Pb SEDEX type deposit, Nordland, Norway. Norges geologiske undersøkelse report 95.154

Morey AA, Tomkins AG, Bierlein FG, Weinberg RF, Davidson GJ (2008) Bimodal distribution of gold in pyrite and arsenopyrite: examples from the Archean Boorara and Bardoc shear zones, Yilgarn Craton, Western Australia. Econ Geol 103:599–614

Mumin AH, Fleet ME, Chryssoulis SL (1994) Gold mineralization in As-rich mesothermal gold ores of the Bogosu-Prestea mining district of the Ashanti Gold Belt, Ghana: remobilization of "invisible" gold. Mineral Deposita 29:445–460

Murakami H, Ishihara S (2013) Trace elements of Indium-bearing sphalerite from tin-polymetallic deposits in Bolivia, China and Japan: a femto-second LA-ICPMS study. Ore Geol Rev 53:223–243

Nutman AP, Ehlers K (1998) Evidence for multiple Palaeoproterozoic thermal events and magmatism adjacent to the Broken Hill Pb–Zn–Ag orebody, Australia. Precambr Res 90:203–238

Oberthür T, Weiser T, Amanor JA, Chryssoulis SL (1997) Mineralogical siting and distribution of gold in quartz veins and sulfide ores of the Ashanti mine and other deposits in the Ashanti belt of Ghana: genetic implications. Mineral Deposita 32:2–15

Page RW, Sweet IP (1998) Geochronology of basin phases in the western Mt Isa Inlier, and correlation with the McArthur Basin. Aust J Earth Sci 45:219–232

Page RW, Conor CHH, Stevens BPJ, Gibson GM, Priess WV, Southgate PN (2005) Correlation of Olary and Broken Hill Domains, Curnamona province: possible relationship to Mount Isa and other North Australian Pb-Zn-Ag-bearing successions. Econ Geol 100: 663–676

Painter MGM, Golding SD, Hannan K, Neudert MK (1999) Sedimentologic, petrographic and sulfur isotope constraints on fine-grained pyrite formation at the Mount Isa mine and environs, northwest Queensland, Australia. Econ Geol 94:883–912

Parr JM, Plimer IR (1993) Models for Broken Hill-type lead–zinc–silver deposits. In: Kirkham RV, Sinclair WD, Thorpe RI, Duke JM (eds) Mineral Deposit Modeling. Geol Assoc Canada Spec Paper 40: p 253–288

Pattrick RAD, Dorling M, Polya DA (1993) TEM study of indium- and copper-bearing growth-banded sphalerite. Can Mineral 31:105–117
Pattrick RAD, Mosselmans JFW, Charnock JM (1998) An x-ray absorption study of doped sphalerites. Eur J Mineral 10:239–249
Perkins WG (1984) Mount Isa silica-dolomite and copper orebodies: the result of a syntectonic hydrothermal alteration system. Econ Geol 79:601–637
Perkins WG (1997) Mount Isa lead-zinc orebodies: replacement lodes in a zoned syndeformational copper-lead-zinc system? Ore Geol Rev 12:61–110
Perkins WG, Bell TH (1998) Stratiform replacement lead-zinc deposits: a comparison between Mount Isa, Hilton, and McArthur River. Econ Geol 93:1190–1212
Phillips GN, Archibald NL, Wall VJ (1985) Metamorphosed high-Fe tholeiites: their alteration and relationships to sulfide mineralization, Broken Hill, Australia. Trans Geol Soc S Afr 88:48–59
Pidgeon RT (1967) A rubidium-strontium geochronological study of the Willyama Complex, Broken Hill, Australia. J Petrol 8:283–324
Plimer IR (1979) Sulphide rock zonation and hydrothermal alteration at Broken Hill, Australia. Trans Inst Min Metall 88:B161–B176
Plimer IR (2007) The world's largest Zn–Pb–Ag deposit: a re-evaluation of Broken Hill (Australia). In: Andrew CJ et al (eds) Mineral deposits: digging deeper. Irish Assoc Econ Geol, Dublin, pp 1239–1242
Polito PA, Kyser TK, Southgate PN, Jackson MJ (2006) Sandstone diagenesis in the Mount Isa basin: an isotopic and fluid inclusion perspective in relationship to district-wide Zn, Pb, and Cu mineralization. Econ Geol 101:1159–1188
Ramberg IB (1967) Geology of the Kongsfjell area, Helgeland, Northern Norway, a petrographic and structural investigation. Bull Nor Geol Unders 240:1–152 (in Norwegian)
Roberts D, Gee DG (1985) An introduction to the structure of the Scandinavian Caledonides. In: Gee DG, Sturt BA (eds) The Caledonide Orogen, Scandinavia and related areas. Wiley, London, pp 55–68
Roberts D, Wolff FC (1981) Tectonostratigraphic development of the Trondheim Region Caledonides. J Struct Geol 3:487–494
Rosenberg JL, Spry PG, Jacobson CE, Cook NJ, Vokes FM (1998) Thermobarometry of the Bleikvassli Zn-Pb-(Cu) deposit, Nordland, Norway. Mineral Deposita 34:19–34
Rothery E (2001) Tectonic origin of the shape of the Broken Hill lodes supported by their structural setting in a high grade shear zone. Aust J Earth Sci 48:201–220
Rui IJ (1972) Geology of the Røros district south-eastern Trondheim region with a special study of the Kjøliskarvene-Holtsjøen area. Nor Geol Tidsskr 52:1–21
Saager R (1967) Drei Typen von Kieslagerstätten im Mofjell-Gebiet, Nordland und ein neuer Vorschlag zur Gliederung der Kaledonischen Kieslager Norwegens. Nor Geol Tidsskr 8:68–73
Schwartz MO (2000) Cadmium in zinc deposits: economic geology of a polluting element. Int Geol Rev 42:445–469
Scott SD (1973) Experimental calibration of the sphalerite geobarometer. Econ Geol 68:466–474
Scott SD, Barnes HL (1971) Sphalerite geothermometry and geobarometry. Econ Geol 66:653–669
Skauli H, Bjørlykke A, Thorpe RI (1992a) Lead-isotope study of the sulphide ore and alteration zone, Bleikvassli zinc-lead deposit, northern Norway. Mineral Deposita 27:276–283
Skauli H, Boyce AJ, Fallick AE (1992b) A sulphur isotopic study of the Bleikvassli Zn-Pb-Cu deposit, Nordland, northern Norway. Mineral Deposita 27:284–292
Smith WD (2000) Genesis of the Mount Isa base metal deposit. Proc Austr Inst Min Metall 1:45–56
Sombuthawee C, Bonsall SB, Hummel FA (1978) Phase-equilibria in systems ZnS-MnS, ZnS-$CuInS_2$, and MnS-$CuInS_2$. J Solid State Chem 25:391–399
Southgate PN, Kyser TK, Scott DL, Large RR, Golding SD, Polito PA (2006) A Basin system and fluid-flow analysis of the Zn-Pb-Ag Mount Isa-Type deposits of Northern Australia: identifying metal source, Basinal Brine Reservoirs, times of fluid expulsion, and organic matter reactions. Econ Geol 101:1103–1115
Spry PG, Marshall B, Vokes FM (eds) (2000) Metamorphosed and metamorphogenic deposits. Rev Econ Geol 11: 310 pp
Spry PG, Heimann A, Messerly J, Houk RS (2007) Discrimination of metamorphic and metasomatic processes at the Broken Hill Pb–Zn–Ag deposit, Australia: rare earth element signatures of garnet-rich rocks. Econ Geol 102:471–494
Spry PG, Plimer IR, Teale GS (2008) Did the giant Broken Hill (Australia) Zn-Pb-Ag deposit melt? Ore Geol Rev 34:223–241
Stanton RL (1963) Constitutional features of the Mount lsa sulfide ores and their interpretation. Proc Aust Inst Min Metall 205:31–153
Stanton RL (1964) Mineral interfaces in stratiform ores. Trans Inst Min Metall 74:45–79
Stanton RL, Russell RD (1959) Anomalous leads and the emplacement of lead sulphide ores. Econ Geol 54:588–607
Stephens MB, Gustavson M, Ramberg IB, Zachrisson E (1985) The Caledonides of north-central Scandinavia ± a tectono-stratigraphic overview. In: Gee DG, Sturt BA (eds) The Caledonide orogen ± Scandinavia and related areas. John Wiley & Sons, New York, pp 135–162
Stevens BPJ, Barnes RG, Brown RE, Stroud WJ, Willis IL (1988) The Willyama Supergroup in the Broken Hill and Euriowie Blocks, New South Wales. Precambr Res 40(41):297–327
Stillwell FL (1959) Petrology of the Broken Hill lode and its bearing on ore genesis. Proc Aust Inst Min Metall 190:1–84
Stüwe K, Ehlers K (1997) Multiple metamorphic events at Broken Hill, Australia. Evidence from Chloritoid-bearing paragenesis in the Nine-Mile Mine region. J Petrol 38:1167–1186
Tauson VL, Chernyshev LV, Makeev AB (1977) Phase relations and structural peculiarities of mixed-crystals in ZnS-MnS system. Geokhimiya 679–692
Vaughan DJ, Craig JR (1978) The mineral chemistry of metal sulfides. Cambridge University Press, Cambridge, 493 pp
Vokes FM (1963) Geological studies on the Caledonian pyritic zinc-lead orebody at Bleikvassli, Nordland, Norway. Nor Geol Unders 222:1–126
Vokes FM (1966) On the possible models of origin of the Caledonian sulfide ore deposit at Bleikvassli, Nordland, Norway. Econ Geol 61: 1130–1139
Vokes FM (1969) A review of metamorphism of sulphide deposits. Earth Sci Rev 5:99–143
Vokes FM (1976) Caledonian massive sulphide deposits in Scandinavia—a comparative review. In: Wolf KH (ed) Handbook of Strata-bound and stratiform ore deposits. Elsevier, Amsterdam, pp 318–329
Vokes FM, Grenne T, Ihlen PM (2003) Caledonian stratabound base-metal sulphides in Scandinavia. In: Kelly JG, Andrew CJ, Ashton JH, Boland MB, Earls G, Fusciardi L, Stanley G (eds) Europe's major base metal deposits. Irish Assoc. Econ. Geol. p 101–126
Wagner T, Klemd R, Wenzel T, Mattson B (2007) Gold upgrading in metamorphosed massive sulfide ore deposits: direct evidence from laser-ablation–inductively coupled plasma–mass spectrometry analysis of invisible gold. Geology 35:775–778
Webster AE (2006) The geology of the Broken Hill lead-zinc-silver deposit, New South Wales, Australia. ARC Centre of Excellence in Ore Deposits (CODES), CODES Monograph 1: 278 pp
Wilde AR, Jones PA, Gessner K, Aillères L, Gregory MJ, Duncan RJ (2006) A geochemical process model for the Mount Isa copper orebodies. Econ Geol 101:1547–1567
Wilson SA, Ridley WI, Koenig AE (2002) Development of sulfide calibration standards for the laser ablation inductively-coupled

plasma mass spectrometry technique. J Anal Atomic Spectrom 17: 406–409

Winderbaum L, Ciobanu CL, Cook NJ, Paul M, Metcalfe A, Gilbert S (2012) Multivariate analysis of an LA-ICP-MS trace element dataset for pyrite. Mathem Geosci 44:823–842

Wolff FC (1967) Geology of the Meraker area as a key to the eastern part of the Trondheim region. Nor Geol Unders 254: 123–146

Woodhead JD, Hellstrom J, Hergt JM, Greig A, Maas R (2007) Isotopic and elemental imaging of geological materials by laser ablation inductively coupled plasma-mass spectrometry. Geostand Geoanal Res 31:331–343

Ye L, Cook NJ, Ciobanu CL, Liu Y, Zhang Q, Liu T, Gao W, Yang Y, Danyushevskiy L (2011) Trace and minor elements in sphalerite from base metal deposits in South China: a LA-ICPMS study. Ore Geol Rev 39:188–217

Ye L, Cook NJ, Liu TG, Ciobanu CL, Gao W, Yang YL (2012) The Niujiaotang Cd-rich zinc deposit, Duyun, Guizhou province, southwest China: ore genesis and mechanisms of cadmium concentration. Mineral Deposita 47:683–700